J. At. Mol. Sci.
doi: 10.4208/jams.022310.031210a

Vol. **1**, No. 3, pp. 253-261
August 2010

An EAM potential for the dynamical simulation of Ni-Al alloys

Jian-Hua Zhang, Shun-Qing Wu, Yu-Hua Wen, and Zi-Zhong Zhu*

Department of Physics and Institute of Theoretical Physics and Astrophysics, Xiamen University, Fujian 361005, China

Received 23 Feburary 2010; Accepted (in revised version) 12 March 2010
Published Online 28 June 2010

Abstract. An embedded atom method potential for Ni-Al alloys is developed. The expression of the embedded function is constructed by analogy with the density function theory. Both the repulsive function and the electron density function here have simple forms. The potential parameters of pure Al and Ni are fitted to the experimental values, including their lattice parameters, cohesive energies, vacancy formation energies and three elastic constants (c_{11},c_{12},c_{13}). The potential for the Ni-Al alloy are then constructed from the Ni and Al potentials. The equation of states and the phonon dispersion calculated by the present potential parameters are in good agreements with first-principles calculations and experimental data, indicating the reliability of the present potential.

PACS: 31.15.Qg, 71.15.Pd, 61.43.-j

Key words: embedded atom method, potential, Al-Ni alloy.

1 Introduction

In the atomic-scale simulation of materials, the first-principles calculations are restricted to a small number of atoms and short time scale. On the other hand, the empirical and semi-empirical methods are very efficient for larger systems and longer time scale. The embedded-atom method (EAM) [1–3], which was developed by Daw and Baskes over two decades ago, has been widely applied in large molecular dynamic simulations because of its computational simplicity. The predictions using EAM for metals have generally been quite good, both qualitatively and quantitatively superior to the early pair potential calculations.

*Corresponding author. *Email address:* zzhu@xmu.edu.cn (Z. Z. Zhu)

In the embedded atom method, the energy required to place an impurity atom in a lattice is taken solely as a function of the electron density at that particular site. Each atomic species therefore has a unique energy function which is in turn a function of just the electron density. However, the theory leads to non-unique EAM potential functions. Different EAM potential functions have been presented [4–13], some with no reference to their physical meaning. In this paper, new EAM potentials for fcc metals Ni, Al and their alloys are constructed. The embedded function in the present work is constructed by analogy with the density function theory and simple forms for the electron density function and the repulsive function are given.

2 Formalism

Under EAM formalism, the total energy is represented as

$$U_{tot}=\frac{1}{2}\sum_{i,j(i\neq j)}\Phi(R_{ij})+\sum_{i}F[\rho_i], \tag{1}$$

where Φ is the pair potential between atoms i and j, $F(\rho_i)$ is the embedded function which is the energy to embed an atom i in an electron density ρ_i. R_{ij} is the separation between atoms i and j, and, ρ_i denotes the host electron density at atom i due to all the other atoms. The host electron density is assumed to be a linear superposition of contributions from individual atoms, and it is given by

$$\rho_i=\sum_{i\neq j}f_i(r_{ij}), \tag{2}$$

where $f_i(r_{ij})$ is the electron density of atom j as a function of distance from its center.

As indicated in the previous section, the EAM potential is not unique. Different forms of $F(\rho_i)$, Φ and $f_i(r_{ij})$ can be presented. Here, we present a new form for the embedded function F by analogy with the density functional theory in order to understand its physical meaning. The density-functional expression for the cohesive energy of a solid is [14]

$$U_{tot}=\frac{1}{2}\sum_{i,j(i\neq j)}\frac{Z_iZ_j}{R_{ij}}+\sum_i\int\frac{\rho(\vec{r})}{|\vec{r}-\vec{R}_i|}d\vec{r}+\frac{1}{2}\iint\frac{\rho(\vec{r})\rho(\vec{r'})}{|\vec{r}-\vec{r'}|}d\vec{r}d\vec{r'}+E_{xc}[\rho]+T_e[\rho] \tag{3}$$

where the first term in the right side of Eq. (3) is the core-core repulsion potential, the second term is the electron-core coulomb interaction, the third term is the electron-electron coulomb interaction, the fourth term is the exchange and correlation energy, and, the fifth term is the electronic kinetic energy. According to Daw [3], the kinetic and exchange-correlation energy density is

$$g(\rho)=t(\rho)+x(\rho)+c(\rho),$$

where the kinetic energy density can be given by [15]

$$t(\rho)=\frac{3}{10}\left[\frac{3}{\pi^2}\right]^{2/3}\rho^{\frac{5}{3}}+\frac{\lambda}{8}\frac{|\nabla\rho|^2}{\rho}, \tag{4}$$

the exchange energy density can be written as

$$x_\rho=-\frac{3}{4}\left[\frac{3}{\pi}\right]^{1/3}\rho^{4/3}, \tag{5}$$

and the correlation energy density is approximated as

$$c(\rho)=\rho\left[-0.0575+0.0155\ln\left(\frac{3}{4\pi\rho}\right)^{1/3}\right]. \tag{6}$$

Neglect the second term of Eq. (4), we rewrite it approximately as

$$t(\rho)=\frac{3}{10}\left[\frac{3}{\pi^2}\right]^{2/3}\rho^{5/3}. \tag{7}$$

For the electron-core and electron-electron coulomb interaction, here, we approximate their energy densities as follows

$$\sum_i\int\frac{\rho(\vec{r})}{|\vec{r}-\vec{R}_i|}d\vec{r}\sim c_2\rho \tag{8}$$

and

$$\frac{1}{2}\iint\frac{\rho(\vec{r})\rho(\vec{r'})}{|\vec{r}-\vec{r'}|}d\vec{r}d\vec{r'}\sim c_3\rho^2. \tag{9}$$

Taking references to Eqs. (4)-(9), we approximated the embedded function as

$$F(\rho)=c_2\rho+c_3\rho^2+c_4g(\rho), \tag{10}$$

with

$$g(\rho)=c_6\rho^2+x(\rho)+c(\rho)=\frac{3}{10}\left(\frac{3}{\pi^2}\right)^{2/3}\rho^{5/3}-\frac{3}{4}\left(\frac{3}{\pi}\right)^{1/3}\rho^{4/3}$$
$$+\left[-0.0575\rho+0.0155\rho\ln\left(\frac{3}{4\pi\rho}\right)^{1/3}\right]$$

It is interesting to compare the present embedded function F with

$$F(\rho)=c_2\rho+c_1\rho+c_8\rho^{5/3}/(c_9+\rho)$$

which was proposed by Angelo *et al*. [16], the only difference is in the approximation of $g(\rho)$.

In brief, the embedded function F is now written as

$$F[\rho]=c_2\rho+c_3\rho^2+c_4\left[0.73856\rho^{4/3}-0.13562\rho^{5/3}+(0.0649\rho+0.00517\rho\ln\rho)\right], \tag{11}$$

with three fitting parameters c_2, c_3 and c_4.

For the repulsive function $\Phi(R_{ij})$, we take a simple form

$$\Phi(R_{ij})=\frac{c_1}{\exp\left(\alpha\left(R_{ij}/r_c-1\right)\right)-1}, \tag{12}$$

with three fitting parameters c_1, α and r_c. For the local electron density function $f(r_{ij})$, we take

$$f(r)=f_e r^n\exp(-\beta r), \tag{13}$$

where f_e is a scaling constant. The format of $f(r)$ is derived from the ground state wave function of the atom. As mentioned by Chen *et al*. [17], the factor r^n can describe approximately the situation that the valence electrons can spread to a larger range in metals. In summary, from Eqs. (10)-(12), we now have 9 parameters $\{n, r_c, f_e, \alpha, \beta, c_1, c_2, c_3, c_4\}$ for the present EAM potential, for a single crystal such as Ni or Al.

For the ordered Ni-Al alloys, the EAM energy expression is [9]

$$E_i=\frac{1}{2}\sum_j\phi_{t_it_j}(r_{ij})+F_{t_i}(\rho_i), \tag{14}$$

where the subscripts t_i and t_j indicate atomic types. Now the core-core repulsion potential ϕ depends on the types of atom i and j. For binary Ni-Al alloys, it is necessary to define the $\phi_{NiNi}(r)$, $\phi_{NiAl}(r)$ and $\phi_{AlAl}(r)$. Except for $\phi_{NiAl}(r)$, $\phi_{NiNi}(r)$, and $\phi_{AlAl}(r)$ are assumed to be transferable from monatomic systems to alloy systems. According to the model of Foiles *et al*. [4], we choose $\phi_{NiAl}(r)$ as follows

$$\phi_{NiAl}(r)=\sqrt{\phi_{NiNi}(r)\phi_{AlAl}(r)}. \tag{15}$$

We therefore do not introduce any other potential parameters for the Ni-Al alloys.

3 Results and discussion

As mentioned in the previous section, we now have 9 parameters $\{n, r_c, f_e, \alpha, \beta, c_1, c_2, c_3, c_4\}$ for the present EAM potential for bulk Ni or Al. In determining these parameters, as usual, the experimental values of lattice constant a_0, cohesive energy E_c, vacancy formation energy E_v^f and three elastic constant (c_{11}, c_{12}, c_{44}) are fitted for bulk fcc Al and Ni, respectively. During the fitting process, we let a_0, E_c and E_v^f equal to the experimental

values. We then minimize the root square deviation between the calculated and experimental values. The optimized parameters obtained from our fittings are listed in Table 1. In Table 2, we show the results of lattice properties calculated from the present EAM parameters along with the experimental data. There is no deviation for a_0 and E_c for Ni and Al, since they are set to equal to the experimental values. As shown in Table 2, the elastic constants and bulk modulus of pure metal Ni are close to the experimental data. However, the fit for bulk Al is not as good as Ni (EAM seemed to describe transition metals better than simple metals). The predictions of lattice constants and cohesive energies for the Ni-Al alloys by the present potential parameters agree within 2% with the experimental data. However, the prediction on some of the elastic constants of NiAl and Ni_3Al are not very good, e.g., the deviations of c_{11} of NiAl and c_{12} of Ni_3Al are 42.1% and 24.1%, respectively. The lack of good transferability to Ni-Al alloys might be due to the simple form we have used in Eq. (14).

To show the reliability of the present EAM potentials, we have calculated the effective

Table 1: The fitted parameters for Ni and Al EAM potentials.

Parameters	Ni	Al
n	1.0	1.0
r_c	1.4	1.6
α	6.60	8.10
β	2.30	1.50
c_1	33.80465244	25.28792441
c_2	65.94077048	33.60140171
c_3	21.50568086	4.97526322
c_4	-114.09767658	-51.65870337
f_e	3.71150806	0.87286555

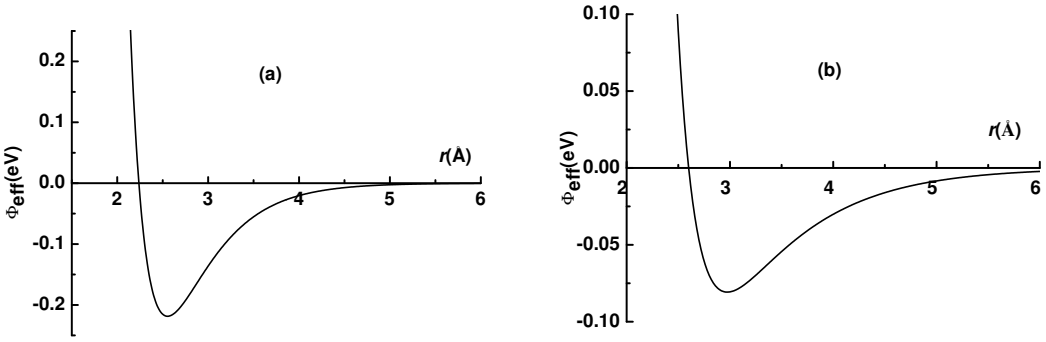

Figure 1: Effective pair potentials for (a) Ni, and (b) Al.

Table 2: Results from present EAM potentials compared with experimental data, for bulk Ni, Al and their ordered alloys NiAl and Ni_3Al.

		a_0 (nm)	E_0 (eV)	c_{11} (GPa)	c_{12} (GPa)	c_{44} (GPa)	B (GPa)
Ni	Expt.	0.3516[a]	4.45[b]	247[b]	147[b]	125[b]	181[b]
	Present	0.3516	4.45	237.85	151.54	129.60	180.31
	Deviation			3.7%	3.1%	3.7%	0.4%
Al	Expt.	0.4032[a]	3.36[b]	114[b]	61.9[b]	31.6[b]	79[b]
	Present	0.4032	3.36	93.19	68.72	35.07	76.88
	Deviation			18.3%	11.0%	11.0%	2.7%
NiAl	Expt.	0.288[c]	4.50[c]	199[c]	137[c]	116[c]	158[e]
	Present	0.2934	4.525	115.14	131.19	124.04	125.84
	Deviation	1.9%	0.6%	42.1%	4.2%	6.9%	20.4%
Ni_3Al	Expt.	0.3567[d]	4.57[d]	230[d]	150[d]	131[d]	177[e]
	Present	0.3578	4.562	196.17	113.80	123.00	141.26
	Deviation	0.3%	0.2%	14.7%	24.1%	6.1%	20.2%

[a] Ref. [22]. The values are at zero temperature, corrected by the data of thermal expansion.

[b] Ref. [11].

[c] Ref. [12].

[d] Ref. [9].

[e] Ref. [23].

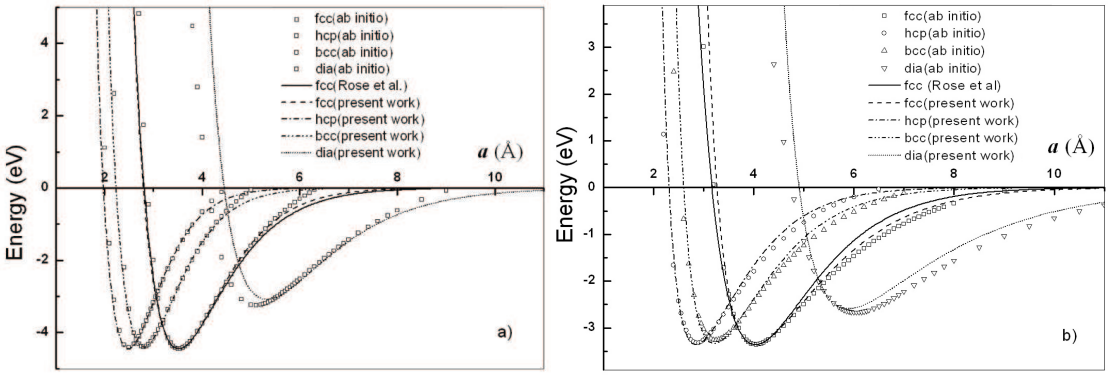

Figure 2: Cohesive energies as a function of lattice constants for various structures, calculated using the present potentials (lines) for (a): Ni, and (b) Al, compared with *ab initio* calculations (dots).

pair potentials which are introduced by Finnis and Sinclair [6] to describe the energy changed associated with any change in configuration of atoms. If the second and higher

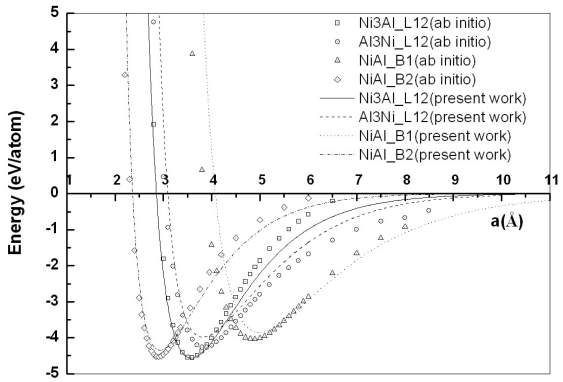

Figure 3: Cohesive energies as a function of lattice constants calculated using the present potentials for various Ni-Al alloys (lines), compared with *ab initio* calculations (dots).

derivatives of F are neglected, the effective pair potential can be defined as

$$\phi_{eff} = \Phi(r) - 2F'(\rho_0)f(r), \tag{16}$$

where $F'(\rho_0)$ is the first derivative of the embedding function. The effective pair potentials for Ni and Al are shown in Fig. 1. As seen in Fig. 1, the effective pair potentials are smooth and very similar to those of the usual empirical pair-potentials.

In order to check the ability of the present EAM potentials for describing the structural stabilities, we compare the equation of states (EOS), i.e., the cohesive energies as a function of the lattice constants, calculated from the first-principles method [18–20] with those from the present EAM parameters. It should be noted that the cohesive energies of the *ab initio* calculations (the minimum points of the curves) are shifted to match the corresponding experimental values of fcc bulk Ni and Al, respectively. EOS's for fcc, bcc, hcp and diamond structures, as well as the EOS from Rose *et al*. [21], are calculated and compared in Fig. 2 for Ni and Al, respectively. Very good agreements of EOS's are shown for fcc, bcc and hcp structures of Ni, with less agreement for the diamond structure which is due to the low-coordination of diamond structure (EAM model might not be able to describe the low-coordination structures well). For Al, generally, the agreements between EAM and first-principles data are also good, with some deviations in the region of large lattice expansions. Fig. 3 compares the equation of states from the present potentials with those from the *ab initio* calculations, for various structures of Ni-Al alloys. Most of the alloy structures by EAM agree well with the *ab initio* calculations around the equilibrium lattice constants. For the $L1_2$-Ni_3Al and B2-NiAl, the EAM and *ab initio* data have some discrepancy at large lattice constants. For B1-NiAl, the difference is more significant. For the order of relative structural stabilities, we show good accord in between the present EAM and the first-principles calculations. The cohesive energies for different structures decrease gradually from Ni_3Al ($L1_2$) $\rightarrow$ NiAl (B2) $\rightarrow$ Al_3Ni (L12) $\rightarrow$ NiAl (B1).

The phonon spectrum gives more information on inter-atomic interaction and is very important in describing the thermodynamic behavior of a material. Therefore, the com-

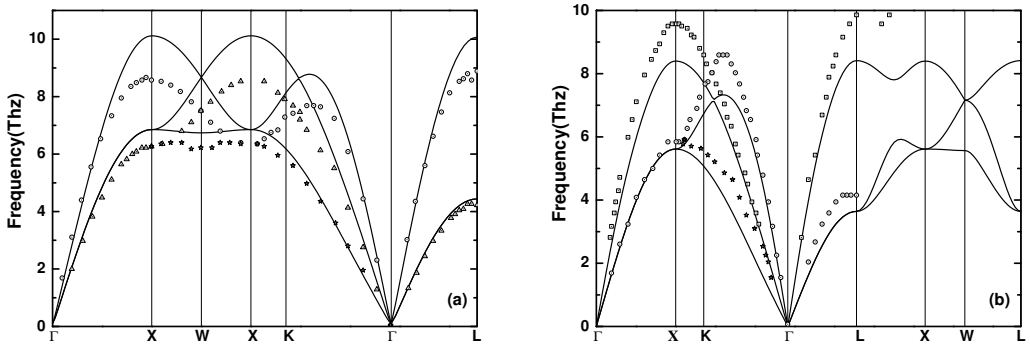

Figure 4: The phonon spectra of (a) fcc Ni and (b) fcc Al. The points are experimental data, taken from Ref. [24] (for Ni) and Ref. [25] (for Al).

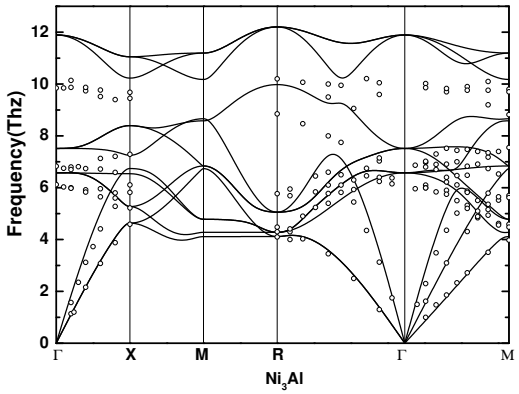

Figure 5: The phonon spectrum of Ni_3Al in $L1_2$ structure. The points are experimental data from Ref. [26].

parison of phonon spectra calculated by the present EAM potentials with experimental data is a crucial test of our EAM model and a good indicator of their predictive abilities. Shown in the Figs. 4 and 5 are the phonon spectra of fcc bulk Ni, Al and their alloy Ni_3Al in the Ll_2 structure. The comparison is in between the present EAM results and the experimental values. Generally speaking, EAM data are in good accord with experimental data in the low energy modes for all the bulk Ni, Al and Ni_3Al. For the higher energy modes, however, the differences between the EAM calculations and experimental data are relatively large. The reason for these disagreements might be due to the fitting of EAM parameters, where the deviations of some elastic constants are relatively large, as shown in Table 2.

4 Conclusions

In conclusion, new EAM potentials for Al, Ni and Ni-Al alloys have been presented. The embedded function was derived by analogy with the density function theory. The

parameters of pure Al and Ni were fitted to the experimental values, including the lattice parameters a_0, the cohesive energies E_c, the vacancy formation energies E_v^f and the elastic constants (c_{11}, c_{12}, c_{44}). The potential of their ordered alloy was then constructed from the potentials of pure Al and Ni. Using these new EAM potentials, the accurate relative stability of different crystal structures have been predicted, as compared to the first-principles calculations. The calculated phonon dispersions of bulk Ni, Al and their alloy Ni_3Al were also in fairly good agreement with measurement.

References

[1] M. S. Daw and M. I. Bakes, Phys. Rev. Lett. 50 (1983) 1285.
[2] M. S. Daw and M. I. Baskes, Phys. Rev. B 29 (1984) 6443.
[3] M. S. Daw, Phys. Rev. B 39 (1989) 7441.
[4] S. M. Foiles, M. I. Baskes, and M. S. Daw, Phys. Rev. B 33 (1986) 7983.
[5] M. I. Baskes, Phys. Rev. B 46 (1992) 2727.
[6] M. W. Finis and J. E. Sinclair, Philos. Mag. A 50 (1984) 45.
[7] R. A. Johnson, Phys. Rev. B 37 (1988) 3924.
[8] R. A. Johnson, Phys. Rev. B 39 (1989) 12554.
[9] A. F. Voter and S. P. Chen, MRS Symp. Proc. 82 (1987) 175.
[10] J. Cai and Y. Y. Ye, Phys. Rev. B 54 (1996) 8398.
[11] Y. Mishin, D. Farka, M. J. Mehl, and D. A. Papaconstantopoulos, Phys. Rev. B 59 (1999) 3393.
[12] Y. Mishin, M. J. Mehl, and D. A. Papaconstantopoulos, Phys. Rev. B 65 (2002) 224114.
[13] Y. Mishin, Acta Mater. 52 (2004) 1451.
[14] P. Hohenberg and W. Kohn, Phys. Rev. 136 (1964) B864.
[15] C. V. von Weizscker, Zeitschrift fur Physik 96 (1935) 431.
[16] J. E. Angelo, N. R. Moody, and M. I. Baskes, Modelling and Simulation in Materials Science and Engineering 3 (1995) 289.
[17] S. Chen, J. Xu, and H. Zhang, Comput. Mater. Sci. 29 (2004) 428.
[18] G. Kresse and J. Hafner, Phys. Rev. B 47 (1993) 558.
[19] G. Kresse and J. Furthmller, Comput. Mater. Sci. 6 (1996) 15.
[20] J. P. Perdew and Y. Wang, Phys. Rev. B 45 (1992) 13244.
[21] J. H. Rose, J. R. Smith, F. Guinea, and J. Ferrante, Phys. Rev. B 29 (1984) 2963.
[22] C. Kittel, Introduction to Solid State Physics (Wiley-Interscience, New York, 1986).
[23] N. Rusovīc and H. Warlimont, Phys. Status Solidi A 44 (1977) 609.
[24] R. J. Birgeneau, J. Cordes, G. Dolling, and A. D. Woods, Phys. Rev. 136 (1964) A1359.
[25] G. Gilat and R. M. Nicklow, Phys. Rev. 143 (1966) 487.
[26] C. Stassis, F. X. Kayser, C. K. Loong, and D. Arch, Phys. Rev. B 24 (1981) 3048.